

## Article

# Improvement of Winter Wheat Aboveground Biomass Estimation Using Digital Surface Model Information Extracted from Unmanned-Aerial-Vehicle-Based Multispectral Images

Yan Guo <sup>1,2,3</sup> , Jia He <sup>1,2</sup>, Huifang Zhang <sup>1,2</sup>, Zhou Shi <sup>4</sup> , Panpan Wei <sup>1,2</sup>, Yuhang Jing <sup>1,2</sup>, Xiuzhong Yang <sup>1,2,3</sup>, Yan Zhang <sup>1,2,3</sup>, Laigang Wang <sup>1,5,\*</sup> and Guoqing Zheng <sup>1,2,3</sup>

<sup>1</sup> Institute of Agricultural Information Technology, Henan Academy of Agricultural Sciences, Zhengzhou 450002, China; 10914063@zju.edu.cn (Y.G.); yzhang1203@hnagri.org.cn (Y.Z.); zgqzx@hnagri.org.cn (G.Z.)

<sup>2</sup> Key Laboratory of Huang-Huai-Hai Smart Agricultural Technology, Ministry of Agriculture and Rural Affairs, Zhengzhou 450002, China

<sup>3</sup> Henan Engineering Research Center of Crop Planting Monitoring and Warning, Zhengzhou 450002, China

<sup>4</sup> Institute of Agricultural Remote Sensing and Information Technology Application, College of Environmental and Resource Sciences, Zhejiang University, Hangzhou 310058, China

<sup>5</sup> International School, Huanghe Science & Technology College, Zhengzhou 450016, China

\* Correspondence: wanglaigang@hnagri.org.cn

**Abstract:** Aboveground biomass (AGB) is an important indicator for characterizing crop growth conditions. A rapid and accurate estimation of AGB is critical for guiding the management of farmland and achieving production potential, and it can also provide vital data for ensuring food security. In this study, by applying different water and nitrogen treatments, an unmanned aerial vehicle (UAV) equipped with a multispectral imaging spectrometer was used to acquire images of winter wheat during critical growth stages. Then, the plant height ( $H_{\text{dsm}}$ ) extracted from the digital surface model (DSM) information was used to establish and improve the estimation model of AGB, using the backpropagation (BP) neural network, a machine learning method. The results show that (1) the  $R^2$ , root-mean-square error (RMSE), and relative predictive deviation (RPD) of the AGB estimation model, constructed directly using the  $H_{\text{dsm}}$ , are 0.58, 4528.23 kg/hm<sup>2</sup>, and 1.25, respectively. The estimated mean AGB (16,198.27 kg/hm<sup>2</sup>) is slightly smaller than the measured mean AGB (16,960.23 kg/hm<sup>2</sup>). (2) The  $R^2$ , RMSE, and RPD of the improved AGB estimation model, based on AGB/ $H_{\text{dsm}}$ , are 0.88, 2291.90 kg/hm<sup>2</sup>, and 2.75, respectively, and the estimated mean AGB (17,478.21 kg/hm<sup>2</sup>) is more similar to the measured mean AGB (17,222.59 kg/hm<sup>2</sup>). The improved AGB estimation model boosts the accuracy by 51.72% compared with the AGB directly estimated using the  $H_{\text{dsm}}$ . Moreover, the improved AGB estimation model shows strong transferability in regard to different water treatments and different year scenarios, but there are differences in the transferability for different N-level scenarios. (3) Differences in the characteristics of the data are the key factors that lead to the different transferability of the AGB estimation model. This study provides an antecedent in regard to model construction and transferability estimation of AGB for winter wheat. We confirm that, when different datasets have similar histogram characteristics, the model is applicable to new scenarios.

**Keywords:** aboveground biomass; UAV; height; transferability; BP neural network; machine learning



**Citation:** Guo, Y.; He, J.; Zhang, H.; Shi, Z.; Wei, P.; Jing, Y.; Yang, X.; Zhang, Y.; Wang, L.; Zheng, G. Improvement of Winter Wheat Aboveground Biomass Estimation Using Digital Surface Model Information Extracted from Unmanned-Aerial-Vehicle-Based Multispectral Images. *Agriculture* **2024**, *14*, 378. <https://doi.org/10.3390/agriculture14030378>

Academic Editors: Yanjun Yang, Ning Zhang, Chengquan Zhou and Jibo Yue

Received: 10 January 2024

Revised: 19 February 2024

Accepted: 23 February 2024

Published: 27 February 2024



**Copyright:** © 2024 by the authors. Licensee MDPI, Basel, Switzerland. This article is an open access article distributed under the terms and conditions of the Creative Commons Attribution (CC BY) license (<https://creativecommons.org/licenses/by/4.0/>).

## 1. Introduction

Aboveground biomass (AGB) has an important impact on light energy utilization and yield formation, and its accurate estimation is one of the key issues in terrestrial ecology research [1,2]. On the one hand, AGB plays an important role in the global carbon cycle [3,4], and an accurate estimation of AGB could help us grasp the feedback between

climate change and agroecosystem interactions [5]. On the other hand, AGB is closely related to crop yield and production [1,6–8]. Therefore, a timely and accurate estimation of AGB is extremely important for guiding the scientific management and rational utilization of farmland, protecting and enhancing the carbon sink function, and providing important data on food security issues [8–10].

In recent years, there have been an increasing number of studies that use remote sensing technology to estimate AGB [11–14]. However, satellite remote sensing images, which are usually used as data for AGB estimation and retrieval, suffer from low spatio-temporal resolution and interference from atmospheric conditions [15,16]. Proximal hyperspectral imagery has a high spectral resolution, but the process is time-consuming and labor-intensive, which limits its application in large-spatial-scale surveys [17]. Compared to satellite remote sensing and proximal hyperspectral remote sensing, low-altitude UAVs can carry different types of sensors, such as RGB cameras, hyperspectral imagers, and multispectral imagers, according to the specific purpose of the survey being conducted [10,11,15]. UAVs have various advantages, such as simplicity in regard to their operation, strong maneuverability, and the ability to acquire high-resolution images below the clouds. They are better suited to field-scale monitoring and serve as a crucial technique in modern agriculture's move toward quantitative and refined approaches [11,18–20]. At present, AGB estimation with UAV remote sensing in agriculture mainly utilizes RGB and multispectral digital orthophoto maps (DOMs) to extract spectral parameters, which are then used to calculate vegetation indices for model construction. For example, Ma et al. [21] and Lu et al. [22] estimated wheat AGB using UAV digital imagery and found that a combination of image color index and texture features can improve the accuracy of wheat biomass estimation, with the highest  $R^2$  being 0.91. Previous studies have focused on utilizing spectral, textural, and vegetation indices extracted from UAV images to estimate crop AGB through linear modeling or machine learning methods [7,12,23,24]. However, due to the interaction of various factors, such as the crop planting area, crop type, and crop growth stages, during the acquisition of canopy information by UAVs, a saturation phenomenon occurs in the vegetation index, which negatively affects the accuracy of the biomass estimation model, as well as the transferability of the model.

In parallel to DOMs, a digital surface model (DSM) is another key piece of information involving ultra-high-resolution UAV images, which is directly related to crop height [25–27]. For example, Chang et al. [28], Watanabe et al. [29], and Luo et al. [30] used UAVs to acquire digital remote sensing images of maize, sorghum, and other crops, and then adopted a digital terrain model (DTM) and a DSM to estimate the plant height of these crops. Their results indicated that the estimated plant height and the measured plant height had an RMSE that varied between 0.33 and 0.88 m. The rise of real-time kinematic (RTK) and post-processing kinematic (PPK) technologies, in particular, provide UAVs with a more prominent advantage in obtaining plant heights quickly and accurately. Wang et al. [31] showed that their crop surface model (CSM), obtained by correcting the DSM using PPK and RTK technologies, can essentially improve plant height estimation accuracy. Therefore, an increasing number of scholars are utilizing UAV images to extract plant heights for biomass estimation [31–33]. For example, Niu et al. [32] extracted the height of maize directly from point cloud data using the Phantom 4 wizard; the  $R^2$  was 0.90 and 0.82 for the plant height estimation and maize biomass estimation, respectively. Bendig et al. [15], Bareth et al. [34], and Wang et al. [31] reported that combining DSM-extracted plant height information with the vegetation index could improve the estimation accuracy of AGB.

However, the extent of the contribution of DSM information to biomass estimation models and the transferability of such models remain largely unclear. Therefore, in this study, we employed a UAV equipped with a multispectral camera, coupled with RTK technology and ground control points, to obtain remote sensing images and elevation information at different key growth stages of winter wheat. Then, we extracted wheat heights from the data obtained by the UAV during these key growth stages and constructed an AGB estimation model using machine learning regression methods. After that, we

analyzed the transferability of the model under different water treatments, across different years, and at various N levels. Our results are expected to provide critical technical support and a theoretical basis for rapid AGB estimation of winter wheat and phenotype research, as well as crop water and fertilizer decision making.

## 2. Materials and Methods

### 2.1. Study Area and Experimental Design

The experiments were conducted on a state-owned farm in Shangshui County, Zhoukou City, Henan Province, central China (33°33' N, 114°37' E), from 2020 to 2022, with a plot area of approximately 42 m<sup>2</sup>. The region is located in the southern part of a warm temperate zone, with a monsoon semi-humid climate and suitable temperatures for crop growth throughout the year. The test soil is sand ginger black soil. Before sowing, the pH is 7.3 in the surface (0–20 cm) layer, and the soil organic matter, total nitrogen content, available phosphorus content, and available potassium content are 25.0 g/kg, 1.69 g/kg, 22.6 mg/kg, and 139.6 mg/kg, respectively. Using a randomized block experimental design, 5 nitrogen application levels (N0 (0 kg/hm<sup>2</sup>), N6 (90 kg/hm<sup>2</sup>), N12 (180 kg/hm<sup>2</sup>), N18 (270 kg/hm<sup>2</sup>), and N24 (360 kg/hm<sup>2</sup>)) and 2 water treatments (rainfed and irrigated) were set. Each N treatment was repeated 3 times, and the two water treatments were named W0 (rainfed) and W1 (irrigated); the total number of plots was 30 (Figure 1). About 50% of each fertilizer was applied as a base fertilizer, and the remaining 50% of the fertilizer was applied as top-dressing during the jointing stage; the amount of the phosphorus fertilizer was 120 kg/hm<sup>2</sup> and the amount of the potassium fertilizer was 90 kg/hm<sup>2</sup>, both of which were applied at once before sowing.

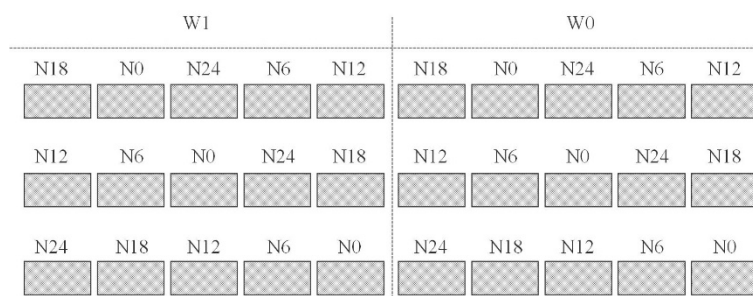


**Figure 1.** Design of the experiment.

### 2.2. Study Framework of AGB Estimation

A general framework of our study is presented in Figure 2. Firstly, a DJ M600 pro UAV was used to acquire UAV remote sensing images during the jointing, flowering, and filling stages of winter wheat, and the images were preprocessed using the Agisoft PhotoScan Professional 12.0 software. During the process of establishing a 3D point cloud, DSM data of the study area were obtained. Then, the height of winter wheat plants in each plot was extracted based on the DSM data. Through an analysis of the relationship between the extracted plant height ( $H_{dsm}$ ), the measured plant height ( $H$ ), and aboveground biomass (AGB), a winter wheat AGB estimation model was established using the BP neural network method. To improve the estimation accuracy, the ratio of AGB to  $H_{dsm}$  was determined to establish the AGB model, and the transferability of the improved model was analyzed across different water treatments, years, and nitrogen treatment scenarios.

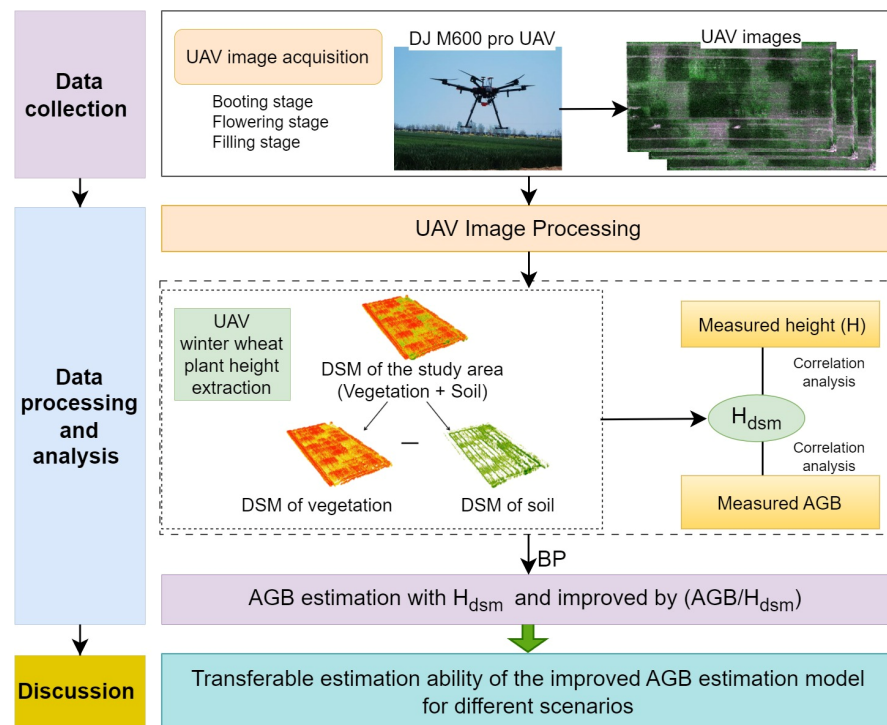


**Figure 2.** Flowchart of the study framework.

### 2.3. Data Acquisition

#### 2.3.1. UAV Platform and Image Acquisition

From 2020 to 2022, during the key growth periods of two winter wheat growth cycles, images were obtained using a DJI M600 Pro UAV equipped with an Anzhou Technology K6 multispectral imager during clear weather from 10:00 to 14:00. The sensor mainly included five bands: a blue band (center wavelength of 450 nm, B), a green band (center wavelength of 550 nm, G), a red band (center wavelength of 685 nm, R), a red-edge band (center wavelength of 725 nm, Rededge), and a near-infrared band (center wavelength of 780 nm, Nir). Four radiometric calibration plates with standard reflectance of 5%, 20%, 40%, and 70% were laid on the ground before the flight. The ground control points (GCPs) of the four vertices and the middle points in the experimental area were measured using a real-time kinematic (RTK) receiver for precise correction of flight position and altitude. The flight altitude was 50 m, and the obtained images had a spatial resolution of 0.02 m.

#### 2.3.2. UAV Image Processing

The preprocessing of UAV data mainly included five steps, namely image format conversion, image filtering, image stitching, orthophoto correction, and radiometric calibration. The details were as follows: (1) The raw MAPIR-format data acquired by K6 was batch converted into TIFF-format data that could be recognized by the Agisoft PhotoScan Professional 12.0 software through the MAPIR Camera Control software. (2) To save time during image stitching, images outside the study area were deleted according to the geographic coordinate information before image stitching. (3) The Agisoft PhotoScan Professional 12.0 software was used for image stitching based on the 3D model mode, which simultaneously obtained orthophoto images and a digital surface model (DSM) of the study area. (4) Based on the RTK geographic information coordinates, the geographic position of the UAV images was accurately corrected. This step could eliminate the positional deviation caused by the fast flight speed. (5) Using the Digital Number (DN) values of the radiometric calibration plates, linear conversion formulas were established to convert the DN values to reflectance values (Table 1). This was performed by assuming that there is a linear relationship between a reflectance value and a DN value:  $y = \text{gain} \times \text{DN} + \text{bias}$ , where  $y$  is the surface

reflectance of a particular band, and gain and bias are the corresponding gain and offset values, respectively. Based on the standard reflectance of the radiometric calibration plates used to establish the relationship with the corresponding pixel DN value, the gain and bias of each band were obtained, and then the DN value was converted to reflectance.

**Table 1.** Reflectance conversion formulas.

| Center Wavelength (nm) | Conversion Formulas                   | R <sup>2</sup> |
|------------------------|---------------------------------------|----------------|
| 450                    | $y = 6.683 \times 10^{-6}DN - 0.0433$ | 0.995          |
| 550                    | $y = 7.207 \times 10^{-6}DN - 0.0728$ | 0.995          |
| 685                    | $y = 7.261 \times 10^{-6}DN - 0.0263$ | 0.999          |
| 725                    | $y = 8.511 \times 10^{-6}DN - 0.0384$ | 0.999          |
| 780                    | $y = 8.812 \times 10^{-6}DN - 0.0506$ | 0.999          |

### 2.3.3. UAV Winter Wheat Plant Height Extraction

The steps of extracting winter wheat plant height ( $H_{dsm}$ ) from UAV images are shown in Figure 3. The process included the following steps: (1) generating point-cloud and aligned photos based on the UAV images; (2) importing ground control points for geometric correction; (3) reconstructing height and output of the crop surface model (CSM); and (4) performing raster calculation to output the winter wheat plant height. Steps (1) to (3) were completed using the Agisoft PhotoScan Professional 12.0 software, and step (4) was completed using the ArcGIS software (version 10.6.1, ESRI). Specifically, bare-ground images were collected on 5 October 2020 for the establishment of a Digital Elevation Model (DEM) of the topography of the study area. During the image stitching process, which aimed to establish the CSM (steps 1 to 4), if the elevation of the ortho-rectified CSM at the control points deviated greatly from the elevation of the measured control points, it was necessary to re-adjust the parameters and re-locate the projection point of the control points on each image before modeling. Therefore, the maximum deviation of the CSM from the measured elevation at the control points was set to be less than 0.01 m, and the CSM could be outputted after achieving this accuracy. The DSM was imported into ArcGIS 10.6 in step (4), and the raster images of the DSM in each growth stage were subtracted from the raster images of the study area’s DEM to obtain a standardized winter wheat CSM. Meanwhile, according to the plot range, a rectangular region of interest (ROI) was drawn. When drawing the ROI, each edge was reserved 1 m from the plot edge to exclude boundary interference. Finally, the plant height of each plot of winter wheat was obtained by partitioning and calculating the statistics of the standardized CSM.

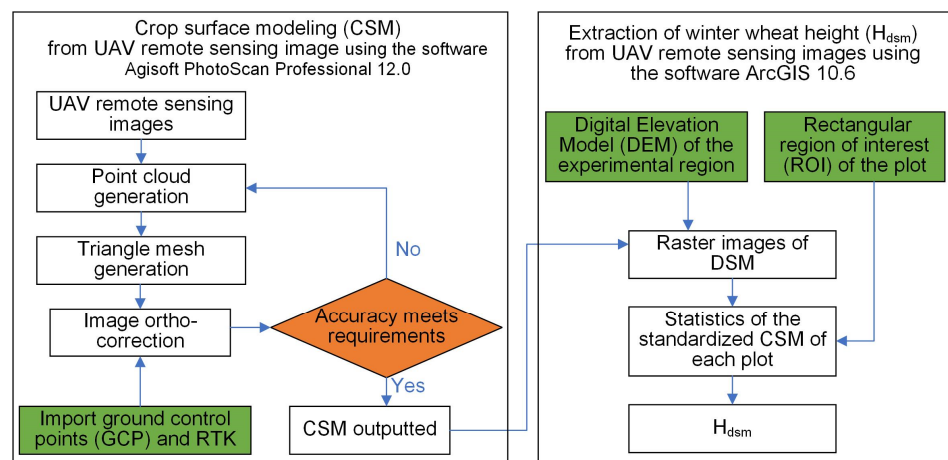


**Figure 3.** Flowchart of the extraction of plant height of winter wheat.

### 2.3.4. Measurement of AGB and Height of Winter Wheat

The acquisition of ground data was synchronized with the acquisition of UAV images. The field samples were collected using a Beidou intelligent handheld terminal (UG908) to obtain the geographic location information of the sampling points. Ten plants with a uniform growth were selected from each plot to measure plant height (H), and the stem samples were packed into sealed bags. The samples were heated for 30 min at 105 °C to halt the metabolic processes, dried at 80 °C in a forced-draft oven, and then weighed to obtain the AGB. A total of 180 samples were obtained.

## 2.4. Methodology

### 2.4.1. AGB Estimation with Backpropagation Neural Network Method

A backpropagation (BP) neural network is a multi-layer feed-forward network that uses error backpropagation for algorithm training; it is one of the most widely used neural network models [35–37]. Currently, there are more than 20 commonly used activation functions for BP neural networks, including identity, sigmoid, and ReLU. When the function identity is active, the input of the node is equal to the output, and it is most suitable for tasks in which the potential behavior is linear [38]. For this reason, we used identity as the activation function of the training model for the nitrogen content of plants. Meanwhile, to prevent overfitting, parameters such as learning rate and regularization were introduced to optimize the model [39]. In this study, a three-layer network structure was designed using a quasi-Newton method family optimizer (lbfgs) to improve the operation speed. Assuming that the output of the hidden layer is set as  $F_j$ , the m-quantity of the output layer is set as  $O_k$ , the excitation function of the system is set as  $G$ , and the learning rate is set as  $\beta$ , the following mathematical relationships can be obtained:

$$\begin{cases} F_j = G\left(\sum_{i=1}^m \omega_{ij}x_i + a_j\right) \\ O_k = \sum_{j=1}^l F_j\omega_{jk} + b_k \end{cases} \quad (1)$$

If the expected output of the system is set to  $T_k$ , the error  $E$  of the system can be expressed by the variance between the actual output value and the expected target value, and the specific relationship is as follows:

$$E = \frac{1}{2} \sum_{k=1}^n (T_k - O_k)^2 \quad (2)$$

Let  $e_k = T_k - O_k$ ; using the principle of gradient descent, the updated formulas of system weights and bias are as follows:

$$\begin{cases} \omega_{ij} = \omega_{ij} + \beta F_j(1 - F_j)x_i \sum_{k=1}^n w_{jk}e_k \\ \omega_{jk} = \omega_{jk} + \beta F_j e_k \end{cases} \quad (3)$$

$$\begin{cases} a_j = a_j + \beta F_j(1 - F_j)x_i \sum_{k=1}^n w_{jk}e_k \\ b_k = b_k + \beta e_k \end{cases} \quad (4)$$

### 2.4.2. Model Metric Evaluation

In this study, three widely used indices—the coefficient of determination ( $R^2$ ), the root-mean-square error (RMSE), and the relative predictive deviation (RPD)—were used to evaluate the model performance. The larger the values of  $R^2$  and PRD and the smaller the RMSE, the better the model performs. When the estimated value matches the measured value perfectly,  $R^2 = 1$  and  $RMSE = 0$ , which indicates strong estimation and transferability of the constructed model. When  $RPD \geq 2$ , it indicates that the model has excellent robust-

ness; when  $1.4 \leq \text{RPD} < 2$ , it indicates that the model has moderate robustness; and when  $\text{RPD} < 1.4$ , it indicates that the robustness of the model is slightly weak [20,40,41]. The formulas are as follows:

$$R^2 = \frac{\sum_{i=1}^n (\hat{y}_i - \bar{y})^2}{\sum_{i=1}^n (y_i - \bar{y})^2} \quad (5)$$

$$\text{RMSE} = \sqrt{\frac{1}{n} \sum_{i=1}^n (\hat{y}_i - y_i)^2} \quad (6)$$

$$\text{RPD} = \sqrt{\frac{\sum_{i=1}^n (y_i - \bar{y})^2}{\sum_{i=1}^n (y_i - \hat{y}_i)^2}} \quad (7)$$

where  $y_i$  and  $\hat{y}_i$  are the measured and predicted biomass of the  $i$ th sample, respectively;  $\bar{y}$  denotes the mean AGB; and  $n$  is the number of samples.

### 3. Results

#### 3.1. Statistical Analysis of Plant Height (H) and Aboveground Biomass (AGB) of Winter Wheat

The changes in H and AGB of winter wheat at different water–N treatments are shown in Figure 4. The W0 and W1 treatments show a gradual increase in both H and AGB with an increase in the N level, but there are variations in the magnitude of the increase. H increases rapidly with an increase in the N level from N0 to N12, while the increase in H from N12 to N24 is smaller. AGB increases quickly with an increase in the N level from N0 to N18; however, a clear difference was detected for the increase in AGB with an increase in the N level from N18 and N24 under different water treatments. Specifically, the AGB of the W0 treatment remains unchanged, while the AGB of the W1 treatment still increases rapidly.

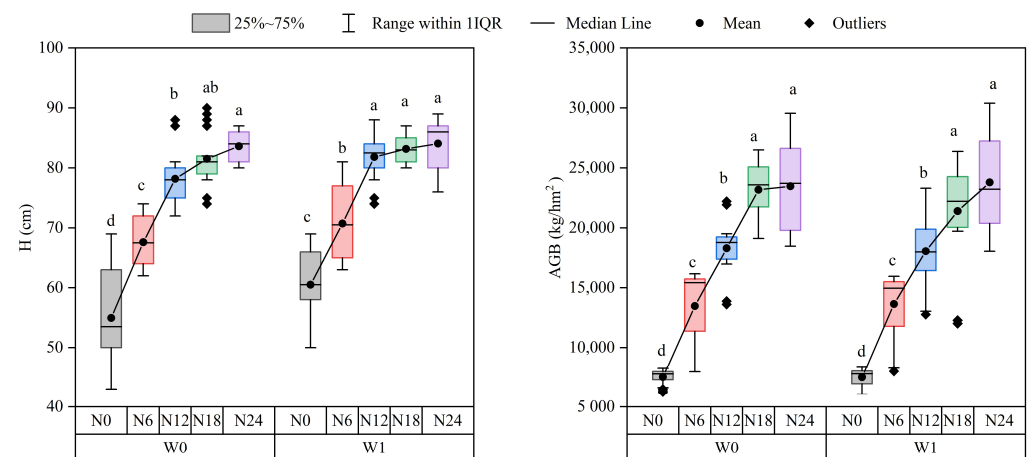


**Figure 4.** H (the left plot) and AGB (the right plot) of winter wheat at different water and nitrogen levels (note: the lowercase letters a, b, c, and d in the figure indicate significant differences at the 0.05 level).

In addition, N treatments can largely affect H and AGB (Figure 1). With an increase in N application, H and AGB increase significantly, but the magnitude of the increase is different. H increases sharply at N levels below N12 and then tends to be stabilized in both W0 and W1 treatments, while AGB continues to sharply increase at N levels above N12 in the W1 treatment. The one-way ANOVA reveals significant differences ( $p < 0.05$ ) for H and AGB with different N levels. The  $t$ -test results also reveal that there are significant differences ( $p < 0.05$ ) for H and AGB under different water treatments. In conclusion, this

study shows that the effect of stress induced by water on H during water–nitrogen coupling is greater than the effect on AGB.

### 3.2. Relationship between $H_{dsm}$ and H under Different Water–N Treatments

The relationship between H estimated by means of DSM ( $H_{dsm}$ ) and the measured H of winter wheat is shown in Figure 5. The correlation between the  $H_{dsm}$  and measured H values declines from 0.59 to 0.07 with an increase in the N level. This is mainly because the change in H tends to become stabilized after N has been applied to a study plot to a certain extent under the same irrigation condition, after which H no longer increases with a further increase in N. Moreover, as presented in Figure 5, the distribution of the  $H_{dsm}$  values is more consistent when the N level increases from N12 to N24, whereas the distribution of H at the N levels of N0 and N6 is relatively dispersed. As the canopy cover of winter wheat increases, winter wheat plants become luxuriant, and three-dimensional structural spatial information of winter wheat may be lacking. Therefore, the errors of the lower boundary and upper boundary of plants caused by the advancement of the growth stage lead to the increase in estimation errors of plant height.

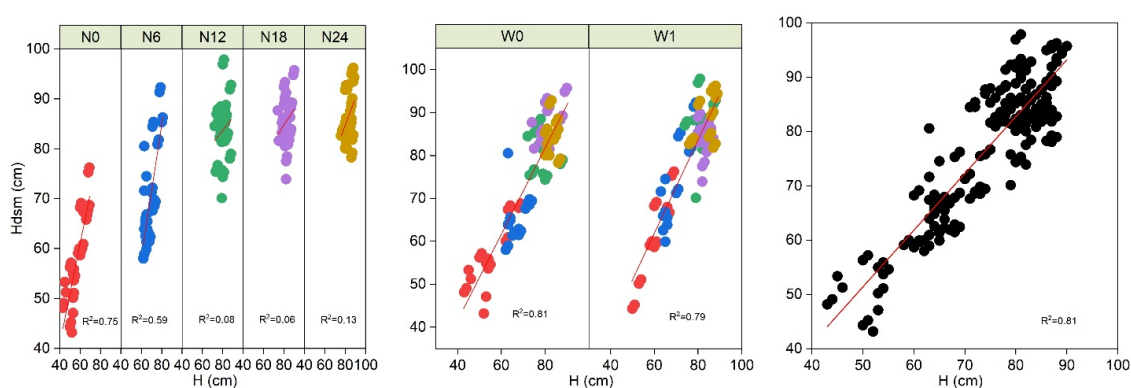


**Figure 5.** Relationship between  $H_{dsm}$  and H under different water–N treatments.

The relationship between  $H_{dsm}$  and H under different water treatments shows that the W0 treatment is superior to the W1 treatment, with  $R^2$  of 0.81 and 0.79, respectively. Combined with Figure 4, this indicates that under the rainfed condition of water–N coupling, the change in H of winter wheat is small, while under the condition of sufficient N, irrigation can increase H. Overall, the linear relationship between  $H_{dsm}$  and H has an  $R^2$  of 0.81, which means that  $H_{dsm}$  can explain more than 80% of the variation in plant height.

### 3.3. Relationship between $H_{dsm}$ and AGB under Different Water–N Treatments

The relationship between the  $H_{dsm}$  and measured AGB values is shown in Figure 6. The correlation between the  $H_{dsm}$  and measured AGB values is not significant as the N level increases. The correlation efficient between the  $H_{dsm}$  and measured AGB values in the W0 treatment ( $R^2 = 0.69$ ) is higher than in the W1 treatment ( $R^2 = 0.50$ ). Combined with Figure 1, it can be concluded that there are differences in the effects of water on AGB and H of winter wheat. This is mainly because when the changes in plant height become stabilized, irrigation causes the increase in biomass to be more likely to manifest as an increase in leaf and stem biomass. Overall, the simple linear relationship model established between  $H_{dsm}$  and AGB has an  $R^2$  of 0.57, which means that  $H_{dsm}$  can explain 57% of the variation in AGB.

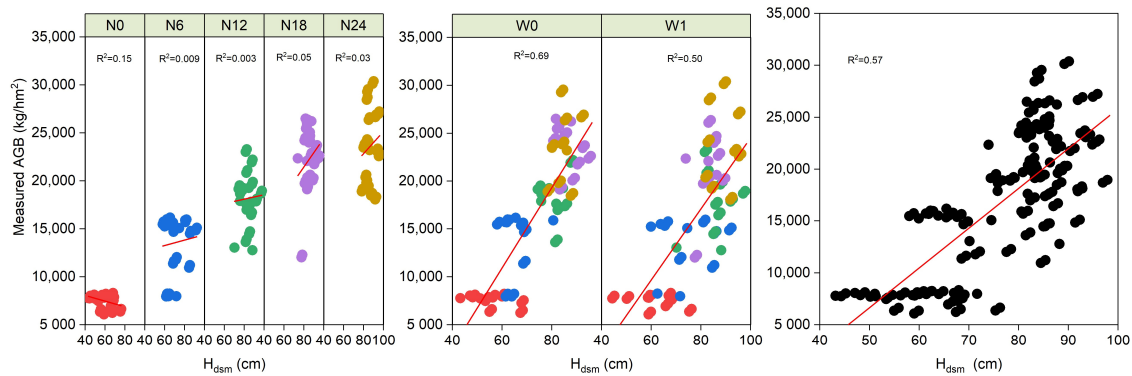


**Figure 6.** Relationship between  $H_{dsm}$  and measured AGB under different water–N treatments.

### 3.4. AGB Estimation Model Construction and Improvement

In the present study, we used the BP method to estimate AGB based on the  $H_{dsm}$  values. The  $R^2$ , RMSE, and RPD of the constructed BP model are 0.58, 4528.23 kg/hm<sup>2</sup>, and 1.25, respectively (Figure 7). The estimated average value of AGB (16,198.27 kg/hm<sup>2</sup>) is smaller than the measured average value (16,960.23 kg/hm<sup>2</sup>), and the estimated values are more dispersed. Generally speaking, the predicted values of AGB are dispersed, with large 95% confidence intervals. The values of  $R^2$ , RMSE, and RPD indicate that the robustness of the model is slightly weak.

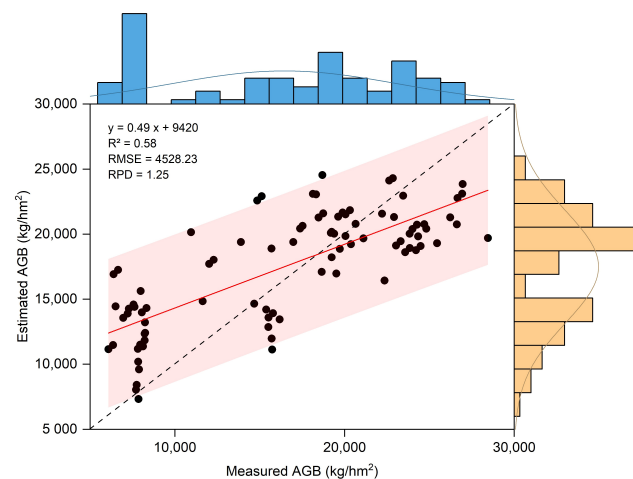


**Figure 7.** Relationship between the measured and estimated AGB based on  $H_{dsm}$ .

Can the estimation ability and robustness of the model be improved by means of data transformation? In this study, we found that the AGB per unit plant height of winter wheat shows an approximately parallel increasing trend with increasing N levels (Figure 8). Based on this relationship, we propose a rapid estimation method of AGB based on the ratio of AGB to  $H_{dsm}$  ( $AGB/H_{dsm}$ ) to improve the estimation accuracy (Figure 9). The AGB was estimated by constructing a model using the same method as described above. The  $R^2$ , RMSE, and RPD of the model based on  $AGB/H_{dsm}$  are 0.88, 2291.90 kg/hm<sup>2</sup>, and 2.75, respectively. The improved model based on  $AGB/H_{dsm}$  could estimate the AGB well, and the estimated mean AGB (17,478.21 kg/hm<sup>2</sup>) is very close to the measured mean AGB (17,222.59 kg/hm<sup>2</sup>). The improved model based on  $AGB/H_{dsm}$  (Figure 9) outperforms the model described in Section 3.4 (Figure 7), with a higher  $R^2$ , a higher RPD, and a lower RMSE. Specifically, the  $R^2$  is improved by 51.72%.

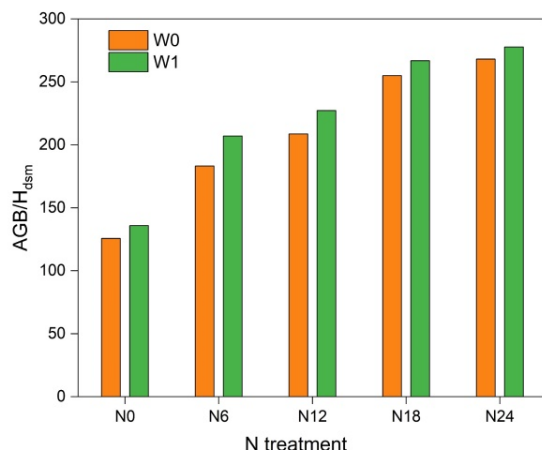


Figure 8. Changing pattern of the ratio AGB to H<sub>dsm</sub> under different water–N treatments.

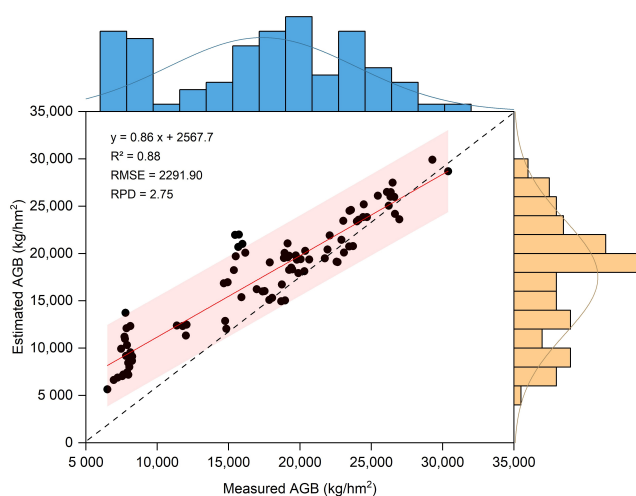


Figure 9. Relationship between measured AGB and estimated AGB according to the model-based ratio.

The improved model assuming a relationship between AGB ( $y$ ) and ratio ( $x$ ) is denoted as  $y = f(x)$ . After the data were substituted into the formula, the model was obtained as  $y = kx - 4004.8$ . Considering the gradually increased AGB across the jointing, flowering, and filling stages, the AGB dataset was intercepted several times to form 10 datasets. The BP method was used for the construction of the AGB estimation model. The relationship between  $k$  and  $H_{dsm}$  is denoted as  $k \approx H_{max}$ , with  $H_{max}$  being the maximum value of  $H_{dsm}$  for each dataset. So, the improved model was transformed for AGB estimation, and the final AGB estimation model can be expressed by the following formula:  $AGB = (4004.80 \times H_{dsm}) / (H_{max} - H_{dsm})$ .

#### 4. Discussion

##### 4.1. Transferability Estimation Ability of the Improved AGB Estimation Model under Different Water Treatments

Based on the W0 and W1 treatment datasets, an AGB estimation model was constructed to validate the transferability estimation of AGB under the W1 treatment and W0 treatment scenarios. The relationships between the measured and estimated AGB under the W1 treatment and the W0 treatment are shown in Figure 10. The model constructed from the W0 treatment dataset was transformed to fit the W1 treatment dataset, with  $R^2$ , RMSE, and RPD of 0.90, 2407.44 kg/hm<sup>2</sup>, and 2.72, respectively. Similarly, the model constructed from the W1 treatment dataset was transformed to fit the W0 treatment dataset, with  $R^2$ , RMSE, and RPD of 0.88, 2496.97 kg/hm<sup>2</sup>, and 2.54, respectively. Overall, the AGB estimation model proposed in this study has high accuracy and robustness, and the models

show improved transferability under different water treatment scenarios in the same study area, which can achieve an accurate and fast estimation of AGB.

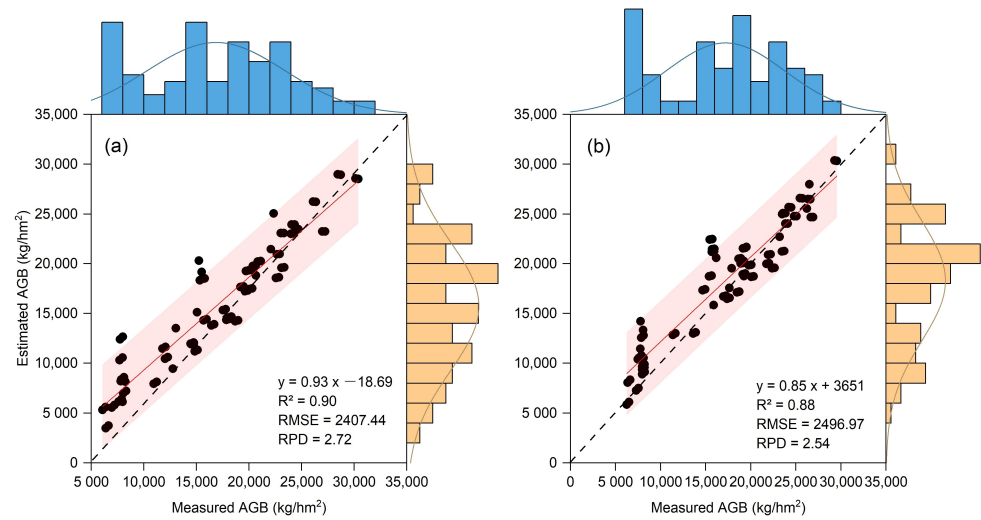


**Figure 10.** The transferability estimation ability of the improved AGB estimation model under different water treatments: (a) the transferability estimation of the W0 model for the W1 treatment, and (b) the transferability estimation of the W1 model for the W0 treatment.

**4.2. Transferability Estimation Ability of the Improved AGB Estimation Model across Different Years**

In this study, the growing season of winter wheat in 2020–2021 was set as  $n$ , and that of 2021–2022 was set as  $n + 1$ . An AGB estimation model was constructed based on the datasets of year  $n$  and  $n + 1$  to validate the transferability estimation of AGB in the context of year  $n + 1$  and year  $n$ . The estimation accuracy of the model for AGB is shown in Figure 11. The model constructed on the data of year  $n$  was transformed to estimate the AGB in year  $n + 1$ , with  $R^2$ , RMSE, and RPD of 0.88, 2257.36 kg/hm<sup>2</sup> and 2.75, respectively. The model constructed from the year  $n + 1$  dataset was transformed to estimate the AGB in year  $n$ , with  $R^2$ , RMSE, and RPD of 0.86, 2239.37 kg/hm<sup>2</sup> and 2.93, respectively. Generally speaking, the AGB estimation model shows good transferability estimation performance between years.

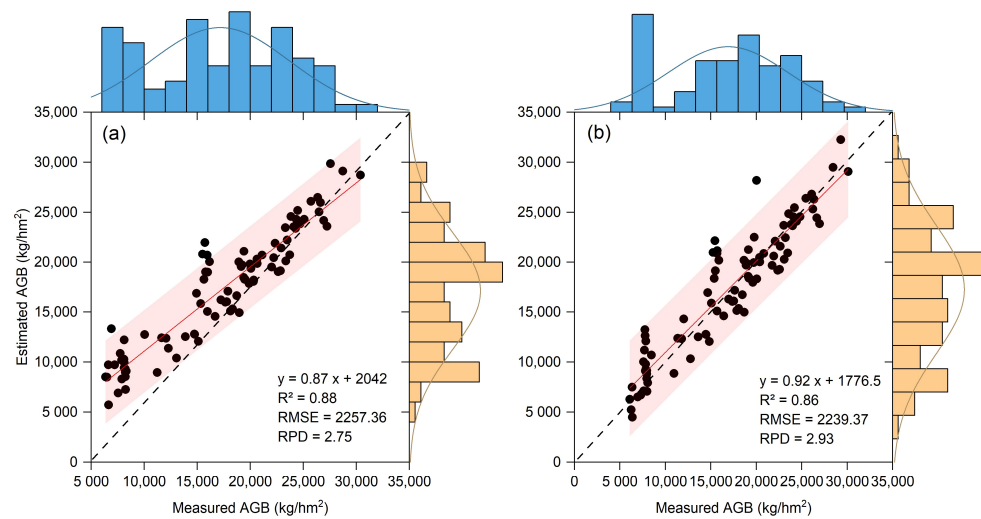


**Figure 11.** The transferability estimation ability of the improved AGB estimation model across different year scenarios: (a) the transferability ability of the  $n$ th-year model to estimate AGB for the  $(n + 1)$ th year, and (b) the transferability ability of the  $(n + 1)$ th-year model to estimate AGB for the  $n$ th year.

#### 4.3. Transferability Estimation Ability of the Improved AGB Estimation Model across Different N Levels

In this part of the study, an AGB estimation model was first constructed based on the N0 dataset, and then it was used to validate the transferability estimation of AGB in the N6, N12, N18, and N24 scenarios. The  $R^2$ , RMSE, and RPD of the model, which was trained using the N0 dataset, are 0.49, 466.91 kg/hm<sup>2</sup>, and 1.49, respectively. When the model was transformed to fit the N6, N12, N18, and N24 scenarios, the model showed bad performance with a large RMSE and a low RPD (Table 2). But the model trained on the N24 dataset had a good performance, with  $R^2$ , RMSE, and RPD of 0.88, 1304.16 kg/hm<sup>2</sup>, and 3.04, respectively. Moreover, the model trained on the N24 dataset also performed well when it was transformed to fit the N12 and N18 scenarios, with a high  $R^2$ , a high RPD, and a low RMSE, which means it has great predictive transferability (Table 2).

**Table 2.** Transferability of the AGB model at different N levels.

| Model Dataset       | $R^2$ | RMSE      | RPD  | Model Datasheet      | $R^2$ | RMSE    | RPD  |
|---------------------|-------|-----------|------|----------------------|-------|---------|------|
| N0_Training dataset | 0.49  | 466.91    | 1.95 | N24_Training dataset | 0.88  | 1304.16 | 3.04 |
| N6_Test dataset     | /     | 5339.59   | 0.61 | N0_test dataset      | /     | 4922.29 | 0.57 |
| N12_Test dataset    | /     | 9370.43   | 0.53 | N6_Test dataset      | /     | 4400.67 | 0.92 |
| N18_Test dataset    | /     | 12,755.63 | 0.53 | N12_Test dataset     | 0.70  | 1402.77 | 1.97 |
| N24_Test dataset    | /     | 13,917.14 | 0.53 | N18_Test dataset     | 0.90  | 1053.85 | 3.06 |

#### 4.4. Factors Affecting the Transferability of Models

In summary, a clear difference was detected regarding the transferability of models trained on datasets for different water treatments, years, and N levels. The models show better transferability across different water treatment and year scenarios, while the transferability of the AGB estimation model across different N levels is not satisfactory. The statistical characteristics of the datasets may play an important role in the transferability of the AGB estimation model. As shown in Figures 12 and 13, the statistical characteristics of the measured AGB and AGB/H<sub>dsm</sub> data are more similar under different water treatments and across different years, with similar values of the means, standard deviations, and other indicators, and the fitted curves basically overlap. But the statistical characteristics of the measured AGB and AGB/H<sub>dsm</sub> are significantly different at different N levels (Figure 14). The datasets of the measured AGB and AGB/H<sub>dsm</sub> at different N levels present different mean values, standard deviations, and other indicators. Combined with Table 2, we can conclude that the statistical characteristics of the employed dataset play an important role in affecting the model's transferability. In this regard, Wang et al. [42] reported that marginal and conditional distributions usually have different contributions to the domain discrepancy. Zhou [39] and Li et al. [43] also argued that transferability is the application of knowledge from one environment to another, and to obtain an ideal transferable prediction model, it requires that the original training dataset not only has a larger amount of data but also a higher data quality so that the model would contain more feature information when transformed to the target model.

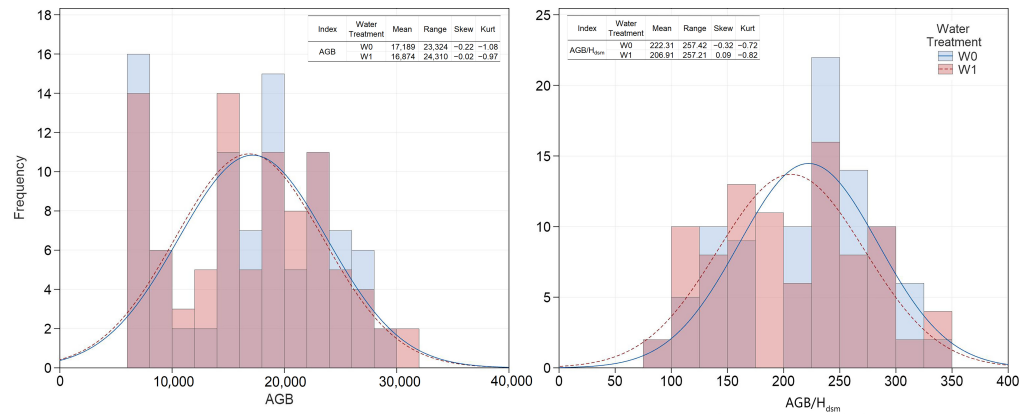


Figure 12. Data characteristics of measured AGB and AGB/H<sub>dsm</sub> under different water treatments.

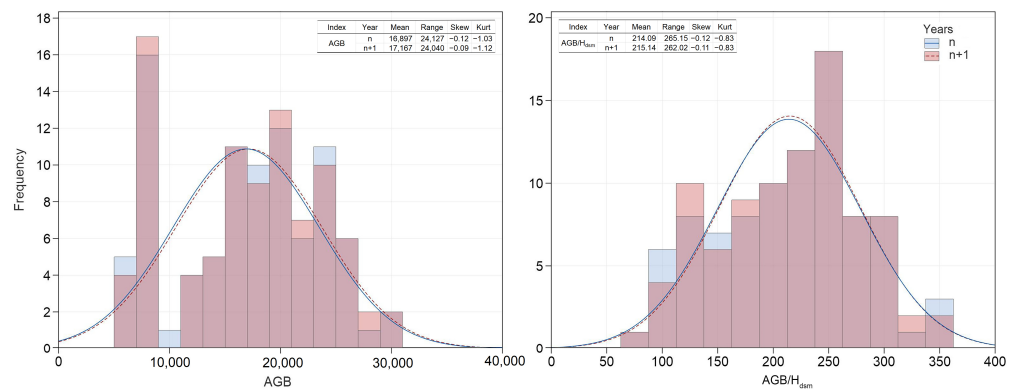


Figure 13. Data characteristics of measured AGB and AGB/H<sub>dsm</sub> across different years.

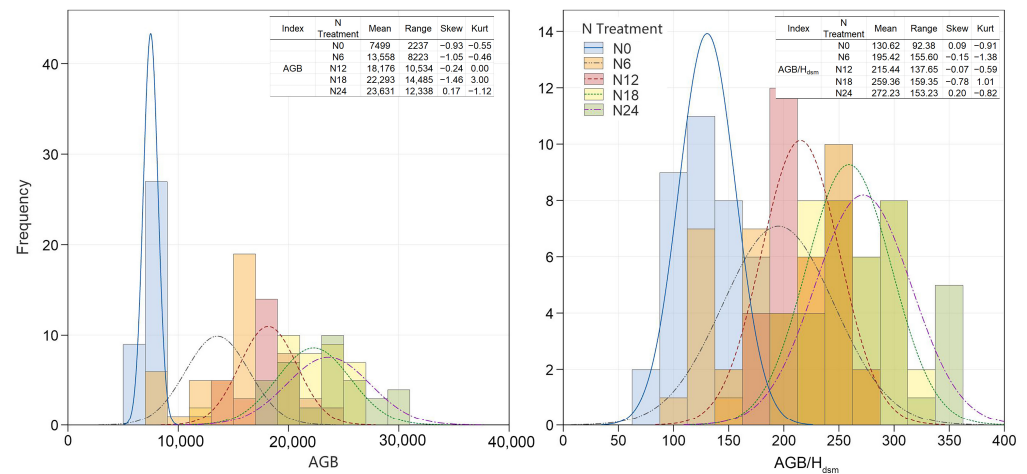


Figure 14. Data characteristics of measured AGB and AGB/H<sub>dsm</sub> at different N levels.

In this study, the transferability of the proposed AGB estimation model was validated under different water treatments, across different years, and at different N levels. The training dataset synthesized information on winter wheat biomass in the study area during several key growth periods. And the results of the statistical analysis of the training dataset and the test dataset were well fitted. Thus, the AGB estimation model has high accuracy and robustness. Our model also shows better transferability across different water treatments and different year scenarios than across different N levels. In practical applications, a targeted selection of pre-trained models for transferability based on the basic characteristics of the data is more helpful in improving model estimation [44].

#### 4.5. Factors Affecting the Accuracy of Models

In this study, the improved winter wheat AGB estimation model based on plant height has an  $R^2$  of 0.88; although its accuracy is lower than the model accuracy of AGB estimation in cases using a combination of vegetation indices, texture features, and other data [23], this model only requires  $H_{\text{dsm}}$  information from UAV remote sensing images, which saves index calculation, texture feature extraction, and other steps, thus presenting the characteristics of simplicity and speed. In addition, Steduto et al. [45] and Han et al. [46] concluded that crop water and other resource utilization is constant during most of the growth period of field crops, and the extraction of a single index based on UAV remote sensing images can be used to estimate AGB; in this regard, this study promotes the efficiency and accuracy of crop biomass estimation based on UAV remote sensing images. However, the use of different methods also has some effects on the estimation results of a model [47]. In this study, the BP neural network method was used to construct the AGB estimation model, and the time taken to train the model was 0.044 s. The parameter settings of the model are shown in Table A1. The  $R^2$  and RMSE of the model for the training dataset are 0.89 and 2099.19 kg/hm<sup>2</sup>, respectively, while the  $R^2$  and RMSE of the model for the test dataset are 0.88 and 2291.90 kg/hm<sup>2</sup>, respectively. Compared with the models developed by Wang et al. [31], the accuracy of the proposed model is better than that of the linear model and the PLSR model, but lower than that of the RF model. This is mainly due to the fact that RF is an ensemble machine learning algorithm wherein multiple indicators are involved and constantly selected when performing model construction, resulting in the improved accuracy of the constructed AGB estimation model, but this method takes more time and increases the complexity of the process when performing the extraction of multiple indicators.

#### 5. Conclusions

In this study, the AGB estimation model of winter wheat was improved by applying different water–N treatments and utilizing plant height information extracted from UAV images. The prediction model for AGB was enhanced by introducing data transformation, and the improved AGB model's  $R^2$ , RMSE, and RPD were 0.88, 2291.90 kg/hm<sup>2</sup>, and 2.75, respectively. Specifically,  $R^2$  was improved by 51.72% compared to that for the model constructed with  $H_{\text{dsm}}$ . Our model shows strong estimation and transferability across different nitrogen levels and different year scenarios, but there are variations in transferability under different nitrogen level scenarios. Differences in the statistical characteristics of the employed datasets are the key factor that leads to different transferability of AGB estimation models. This study provides an antecedent for model construction and transferability estimation, and we found that when different datasets have similar histogram characteristics, the constructed model is applicable to new scenarios. However, we should also note that the AGB is affected by many factors and, thus, the accuracy of its estimation model is also related to many factors such as the representativeness of the samples, the vegetation coverage, and the planting density. In this study, we analyzed the effects of factors such as water, year, and N levels on the accuracy of the AGB estimation model, but when building the estimation model, the methods used also influenced the estimation results of the model. Therefore, expanding the training dataset and considering the influencing factors of the constructed AGB model from multiple perspectives will help to further improve the generalization ability and robustness of the AGB model and increase the practical value of the model.

**Author Contributions:** All authors have made significant contributions to this research. Conceptualization, Y.G., P.W. and Y.J.; writing—original draft preparation, Y.G., J.H., X.Y. and L.W.; experimental design and data curation, Y.J., H.Z., Y.Z. and G.Z.; funding acquisition, Y.G. and L.W.; discussion of results and manuscript revision, Y.G., Z.S. and G.Z. All authors have read and agreed to the published version of the manuscript.

**Funding:** This research was funded by the National Key R&D Special Projects (Grant no. 2022YFD2001105), the Outstanding Youth Program of Henan Academy of Agricultural Sciences (Grant no. 2021JQ02), and the Science and Technology Innovation Leading Talent Cultivation Program of the Institute of Agricultural Information Technology, Henan Academy of Agricultural Sciences (Grant no. 2022KJCX01), the Independent innovation projects of Henan Academy of Agricultural Sciences (Grant no. 2023ZC062), and the Agricultural Remote Sensing Innovation Team, Henan Academy of Agricultural Sciences (Grant no. 2024TD28).

**Institutional Review Board Statement:** Not applicable.

**Data Availability Statement:** The datasets for this manuscript are not publicly available because our team is working on other publications with them and they are not yet ready for sharing. Requests to access the datasets should be directed to Y.G. at 10914063@zju.edu.cn.

**Acknowledgments:** We would like to thank Yongzheng Cheng, Hongli Zhang, and Ting Liu for their help in data collection. The authors also thank the editors and the anonymous reviewers for their suggestions on improving the manuscript.

**Conflicts of Interest:** The authors declare no conflicts of interest.

## Appendix A

In this study, BP was performed using a computer with an Intel Core i7-9700K CPU and 64 GB RAM, and the parameter settings are shown in Table A1.

**Table A1.** Parameters for BP neural network.

| Parameters                            | Parameter Value |
|---------------------------------------|-----------------|
| Training time                         | 0.044 s         |
| Data slicing                          | 0.5             |
| Data shuffling                        | No              |
| Cross-validation                      | 30% of dataset  |
| Activation function                   | identity        |
| Solver                                | lbfgs           |
| Learning rate                         | 0.1             |
| L2 regular term                       | 1               |
| Number of iterations                  | 1000            |
| Number of neurons in 1st hidden layer | 100             |

## References

- Wang, D.; Li, R.; Zhu, B.; Liu, T.; Sun, C.; Guo, W. Estimation of wheat plant height and biomass by combining UAV imagery and elevation data. *Agriculture* **2023**, *13*, 9. [[CrossRef](#)]
- Zeng, L.; Liu, X.; Li, W.; Ou, J.; Cai, Y.; Chen, G.; Li, M.; Li, G.; Zhang, H.; Xu, X. Global simulation of fine resolution land use/cover change and estimation of aboveground biomass carbon under the shared socioeconomic pathways. *J. Environ. Manag.* **2022**, *312*, 114943. [[CrossRef](#)] [[PubMed](#)]
- Piao, S.; Fang, J.; Ciais, P.; Peylin, P.; Huang, Y.; Sitch, S.A.; Wang, T. The carbon balance of terrestrial ecosystems in China. *Nature* **2009**, *458*, 1009–1013. [[CrossRef](#)]
- Bar-On, Y.M.; Phillips, R.; Milo, R. The biomass distribution on Earth. *Proc. Natl. Acad. Sci. USA* **2018**, *115*, 6506–6511. [[CrossRef](#)] [[PubMed](#)]
- Wei, M.; Ma, T.; Cao, M.; Wei, B.; Li, C.; Li, C.; Zhang, K.; Fang, Y.; Sun, X. Biomass estimation and characterization of the nutrient components of thinned unripe grapes in China and the global grape industries. *Food Chem. X* **2022**, *15*, 100363. [[CrossRef](#)] [[PubMed](#)]
- Zheng, Y.; Zhang, M.; Zhang, X.; Zeng, H.; Wu, B. Mapping winter wheat biomass and yield using time series data blended from PROBA-V 100- and 300-m S1 products. *Remote Sens.* **2016**, *8*, 824. [[CrossRef](#)]
- Alabi, T.R.; Abebe, A.T.; Chigeza, G.; Fowobaje, K.R. Estimation of soybean grain yield from multispectral high-resolution UAV data with machine learning models in West Africa. *Remote Sens. Appl.* **2022**, *27*, 100782. [[CrossRef](#)]
- Zhang, J.; Zhao, Y.; Hu, Z.; Xiao, W. Unmanned aerial system-based wheat biomass estimation using multispectral, structural and meteorological data. *Agriculture* **2023**, *13*, 1621. [[CrossRef](#)]
- Delécolle, R.; Maas, S.J.; Guérif, M.; Baret, F. Remote sensing and crop production models: Present trends. *ISPRS J. Photogr.* **1992**, *47*, 145–161. [[CrossRef](#)]

10. Chen, Z.; Wang, J.; Jin, J. Fully automated proximal hyperspectral imaging system for high-resolution and high-quality in vivo soybean phenotyping. *Precis. Agric.* **2023**, *24*, 2395–2415. [[CrossRef](#)]
11. Zhu, W.; Sun, Z.; Peng, J.; Huang, Y.; Li, J.; Zhang, J.; Yang, B.; Liao, X. Estimating maize above-ground biomass using 3D point clouds of multi-source unmanned aerial vehicle data at multi-spatial scales. *Remote Sens.* **2019**, *11*, 2678. [[CrossRef](#)]
12. Imran, A.B.; Khan, K.; Ali, N.; Ahmad, N.; Ali, A.M.; Shah, K. Narrow band based and broadband derived vegetation indices using Sentinel-2 Imagery to estimate vegetation biomass. *Glob. J. Environ. Sci. Manag.* **2020**, *6*, 97–108.
13. Adar, S.; Sternberg, M.; Paz-Kagan, T.; Henkin, Z.; Dovrat, G.; Zaady, E.; Argaman, E. Estimation of aboveground biomass production using an unmanned aerial vehicle (UAV) and VEN $\mu$ S satellite imagery in Mediterranean and semiarid rangelands. *Remote Sens. Appl.* **2022**, *26*, 100753. [[CrossRef](#)]
14. Falcioni, R.; Santos, G.L.A.A.d.; Crusiol, L.G.T.; Antunes, W.C.; Chicati, M.L.; Oliveira, R.B.d.; Demattê, J.A.M.; Nanni, M.R. Non-invasive assessment, classification, and prediction of biophysical parameters using reflectance hyperspectroscopy. *Plants* **2023**, *12*, 2526. [[CrossRef](#)]
15. Bendig, J.; Yu, K.; Aasen, H.; Bolten, A.; Bennertz, S.; Broscheit, J.; Gnyp, M.L.; Bareth, G. Combining UAV-based plant height from crop surface models, visible, and near infrared vegetation indices for biomass monitoring in barley. *Int. J. Appl. Earth Obs. Geoinf.* **2015**, *39*, 79–87. [[CrossRef](#)]
16. Zhou, Y.; Liu, T.; Batelaan, O.; Duan, L.; Wang, Y.; Li, X.; Li, M. Spatiotemporal fusion of multi-source remote sensing data for estimating aboveground biomass of grassland. *Ecol. Indic.* **2023**, *146*, 109892. [[CrossRef](#)]
17. Thomson, A.; Jacobs, J.; Morse-McNabb, E. Comparing the predictive ability of Sentinel-2 multispectral imagery and a proximal hyperspectral sensor for the estimation of pasture nutritive characteristics in an intensive rotational grazing system. *Comput. Electron. Agric.* **2023**, *214*, 108275. [[CrossRef](#)]
18. Zou, M.; Liu, Y.; Fu, M.; Li, C.; Zhou, Z.; Meng, H.; Xing, E.; Ren, Y. Combining spectral and texture feature of UAV image with plant height to improve LAI estimation of winter wheat at jointing stage. *Front. Plant Sci.* **2024**, *14*, 1272049. [[CrossRef](#)]
19. Fu, Y.; Yang, G.; Song, X.; Li, Z.; Xu, X.; Feng, H.; Zhao, C. Improved estimation of winter wheat aboveground biomass using multiscale textures extracted from UAV-based digital images and hyperspectral feature analysis. *Remote Sens.* **2021**, *13*, 581. [[CrossRef](#)]
20. Guo, Y.; He, J.; Huang, J.; Jing, Y.; Xu, S.; Wang, L.; Li, S.; Zheng, G. Effects of the spatial resolution of UAV images on the prediction and transferability of nitrogen content model for winter wheat. *Drones* **2022**, *6*, 299. [[CrossRef](#)]
21. Ma, J.; Li, Y.; Chen, Y.; Du, K.; Zheng, F.; Zhang, L.; Sun, Z. Estimating above ground biomass of winter wheat at early growth stages using digital images and deep convolutional neural network. *Eur. J. Agron.* **2019**, *103*, 117–129. [[CrossRef](#)]
22. Lu, N.; Zhou, J.; Han, Z.; Li, D.H.; Cao, Q.; Yao, X.; Tian, Y.; Zhu, Y.; Cao, W.; Cheng, T. Improved estimation of aboveground biomass in wheat from RGB imagery and point cloud data acquired with a low-cost unmanned aerial vehicle system. *Plant Methods* **2019**, *15*, 17. [[CrossRef](#)] [[PubMed](#)]
23. Luo, S.; Jiang, X.; He, Y.; Li, J.; Jiao, W.; Zhang, S.; Xu, F.; Han, Z.; Sun, J.; Yang, J.; et al. Multi-dimensional variables and feature parameter selection for aboveground biomass estimation of potato based on UAV multispectral imagery. *Front. Plant Sci.* **2022**, *13*, 948249. [[CrossRef](#)] [[PubMed](#)]
24. Singh, R.; Biradar, C.; Behera, M.; Prakash, A.; Das, P.; Mohanta, M.; Krishna, G.; Dogra, A.; Dhyani, S.; Rizvi, J. Optimising carbon fixation through agroforestry: Estimation of aboveground biomass using multi-sensor data synergy and machine learning. *Ecol. Inform.* **2024**, *79*, 102408. [[CrossRef](#)]
25. Xie, T.; Li, J.; Yang, C.; Jiang, Z.; Chen, Y.; Guo, L.; Zhang, J. Crop height estimation based on UAV images: Methods, errors, and strategies. *Comput. Electron. Agric.* **2021**, *185*, 106155. [[CrossRef](#)]
26. Qiu, R.; Zhang, M.; He, Y. Field estimation of maize plant height at jointing stage using an RGB-D camera. *Crop J.* **2022**, *10*, 1274–1283. [[CrossRef](#)]
27. Yang, K.; Mo, J.; Luo, S.; Peng, Y.; Fang, S.; Wu, X.; Zhu, R.; Li, Y.; Yuan, N.; Zhou, C.; et al. Estimation of rice aboveground biomass by UAV imagery with photosynthetic accumulation models. *Plant Phenomics* **2023**, *5*, 0056. [[CrossRef](#)]
28. Chang, A.; Jung, J.; Maeda, M.; Landivar, J. Crop height monitoring with digital imagery from Unmanned Aerial System (UAS). *Comput. Electron. Agric.* **2017**, *141*, 232–237. [[CrossRef](#)]
29. Watanabe, K.; Guo, W.; Arai, K.; Takanashi, H.; Kajiya-Kanegae, H.; Kobayashi, M.; Yano, K.; Tokunaga, T.; Fujiwara, T.; Tsutsumi, N.; et al. High-throughput phenotyping of sorghum plant height using an unmanned aerial vehicle and its application to genomic prediction modeling. *Front. Plant Sci.* **2017**, *8*, 421. [[CrossRef](#)]
30. Luo, S.; Liu, W.; Zhang, Y.; Wang, C.; Xi, X.; Nie, S.; Ma, D.; Lin, Y.; Zhou, G. Maize and soybean heights estimation from unmanned aerial vehicle (UAV) LiDAR data. *Comput Electron Agric.* **2021**, *182*, 106005. [[CrossRef](#)]
31. Wang, F.; Yang, M.; Ma, L.; Zhang, T.; Qin, W.; Li, W.; Zhang, Y.; Sun, Z.; Wang, Z.; Li, F.; et al. Estimation of Above-Ground Biomass of Winter Wheat Based on Consumer-Grade Multi-Spectral UAV. *Remote Sens.* **2022**, *14*, 1251. [[CrossRef](#)]
32. Niu, Y.X.; Zhang, L.Y.; Zhang, H.H.; Han, W.T.; Peng, X.S. Estimating above-ground biomass of maize using features derived from UAV-based RGB imagery. *Remote Sens.* **2019**, *11*, 1261. [[CrossRef](#)]
33. Shu, M.Y.; Li, Q.; Ghafoor, A.; Zhu, J.; Li, B.; Ma, Y. Using the plant height and canopy coverage to estimation maize aboveground biomass with UAV digital images. *Eur. J. Agron.* **2023**, *151*, 126957. [[CrossRef](#)]

34. Bareth, G.; Bendig, J.; Tilly, N.; Hoffmeister, D.; Aasen, H.; Bolten, A. A comparison of UAV- and TLS-derived plant height for crop monitoring: Using polygon grids for the analysis of crop surface models (CSMs). *Photogramm. Fernerkun.* **2016**, *2016*, 85–94. [[CrossRef](#)]
35. Du, B.; Lund, P.D.; Wang, J.; Kolhe, M.L.; Hu, E. Comparative study of modelling the thermal efficiency of a novel straight through evacuated tube collector with MLR, SVR, BP and RBF methods. *Sustain. Energy Technol.* **2021**, *44*, 101029. [[CrossRef](#)]
36. Lan, W.Q.; Yang, X.; Gong, T.S.; Xie, J. Predicting the shelf life of *Trachinotus ovatus* during frozen storage using a back propagation (BP) neural network model. *Aquac. Fish.* **2023**, *8*, 544–550. [[CrossRef](#)]
37. Tang, X.; Liu, H.; Feng, D.; Zhang, W.; Chang, J.; Li, L.; Yang, L. Prediction of field winter wheat yield using fewer parameters at middle growth stage by linear regression and the BP neural network method. *Eur. J. Agron.* **2022**, *141*, 126621. [[CrossRef](#)]
38. Li, H. *Machine Learning Method*; Tsinghua University Press: Beijing, China, 2022. (In Chinese)
39. Zhou, Z.H. *Machine Learning*; Tsinghua University Press: Beijing, China, 2022. (In Chinese)
40. Chang, C.; Laird, D.A.; Mausbach, M.J.; Hurburgh, C.R. Near-infrared reflectance spectroscopy–principal components regression analyses of soil properties. *Soil Sci. Soc. Am. J.* **2001**, *65*, 480–490. [[CrossRef](#)]
41. Mireei, S.A.; Mohtasebi, S.S.; Massudi, R.; Rafiee, S.; Arabanian, A.S.; Berardinelli, A. Non-destructive measurement of moisture and soluble solids content of mazafati date fruit by NIR spectroscopy. *Aust. J. Crop Sci.* **2010**, *4*, 175–179.
42. Wang, J.; Chen, Y.; Feng, W.; Yu, H.; Huang, M.; Yang, Q. Transfer learning with dynamic distribution adaptation. *ACM Trans. Intell. Syst. Technol.* **2019**, *11*, 1–25. [[CrossRef](#)]
43. Li, C.G.; Zhang, B.; Zhao, Q.; Cheng, X.P.; WANG, X.F. Empathy prediction from texts based on transfer learning. *J. Comput. Appl.* **2022**, *42*, 3603–3609. (In Chinese)
44. Zhu, W.; Braun, B.; Chiang, L.H.; Romagnoli, J.A. Investigation of transfer learning for image classification and impact on training sample size. *Chemom. Intell. Lab.* **2021**, *211*, 104269. [[CrossRef](#)]
45. Steduto, P.; Albrizio, R. Resource use efficiency of field-grown sunflower, sorghum, wheat and chickpea: II. Water use efficiency and comparison with radiation use efficiency. *Agric. For. Meteorol.* **2005**, *130*, 269–281. [[CrossRef](#)]
46. Han, W.T.; Tang, J.D.; Zhang, L.Y.; Niu, Y.X.; Wang, T.H. Maize water use efficiency and biomass estimation based on unmanned aerial vehicle remote sensing. *Trans. CSAM* **2021**, *52*, 129–141. (In Chinese)
47. Xu, W.K.; Zhao, L.G.; Li, J.; Shang, X.P.; Ding, X.P.; Wang, T.W. Detection and classification of tea buds based on deep learning. *Comput. Electron. Agric.* **2022**, *192*, 106547. [[CrossRef](#)]

**Disclaimer/Publisher’s Note:** The statements, opinions and data contained in all publications are solely those of the individual author(s) and contributor(s) and not of MDPI and/or the editor(s). MDPI and/or the editor(s) disclaim responsibility for any injury to people or property resulting from any ideas, methods, instructions or products referred to in the content.